Available online at www.sciencedirect.com
SCIENCE DIRECT®
Earth and Planetary Science Letters 241 (2006) 505–516
EPSL
www.elsevier.com/locate/epsl

The penultimate deglaciation: High-resolution paleoceanographic evidence from a north–south transect along the eastern Nordic Seas

Bjørg Risebrobakken [a,b,*], Estelle Balbon [c], Trond Dokken [a], Eystein Jansen [a,b], Catherine Kissel [c], Laurent Labeyrie [c], Thomas Richter [d], Liv Senneset [a]

[a] *Bjerknes Centre for Climate Research, Allégaten 55, 5007 Bergen, Norway*
[b] *Department of Earth Science, University of Bergen, Allégaten 41, 5007 Bergen, Norway*
[c] *Laboratoire des Sciences du Climat et de l'Environnement, Unité de recherche mixte CEA/CNRS, Campus du CNRS, Avenue de la Terrasse, Bat 12, 91198 Gif-sur-Yvette Cedex, France*
[d] *Royal Netherlands Institute for Sea Research, P.O. Box 59, 1790 AB Den Burg, Texel, The Netherlands*

Received 18 March 2005; received in revised form 12 September 2005; accepted 23 November 2005
Available online 4 January 2006
Editor: E. Boyle

Abstract

The penultimate termination has been studied with focus on oceanographic changes in the eastern Nordic Seas and the influence of these changes on the surrounding ice sheets and vice versa. Repeatedly, major changes in the strength of the Atlantic Meridional Overturning Circulation (AMOC) occurred during the studied interval. Times of strong overturning and increased heat transport northwards were of importance in triggering one minor and two major disintegration events. The two major disintegration events were separated by a deglacial pause, characterized by a strong AMOC. The same variability is seen throughout the eastern Nordic Seas, from the Faeroe–Shetland Channel in the south to the Fram Strait in the north. Some of the oceanographic changes occurring during the penultimate termination are comparable with changes seen through the last deglaciation. Reduced winter moisture flux and increased summer melting due to the present insolation forcing further amplified the rate of ice sheet disintegration. Calculated sea-level change through TII shows a mean change of 121 ± 4 m, 41 ± 16 m in the first step and 80 ± 13 m in the last step.

Keywords: deglaciation; AMOC; sea level change; Nordic Seas; multi-proxy approach; melt water; brine

1. Introduction

Through deglaciation the climate system experience major reorganisation, replacing the glacial extreme end-member by the other extreme, interglacial conditions, within a few millennia. Insolation changes are thought to be the major triggering mechanism for glacial terminations [1–3]. However, a number of feedback mechanisms also contribute to the demise of the ice sheets [4–9], thus shaping the overall configuration of the deglaciation. The aim of this paper is to reconstruct the behaviour of the northern limb of the Atlantic Meridional Overturning Circulation (AMOC) through the penultimate deglaciation (Termination II (TII)), and further identify how it influenced the disintegration of the Northern European Ice Sheets. Termination II and I are compared to see if the oceanic reorganisations during the deglaciation are comparable under otherwise

* Corresponding author. Bjerknes Centre for Climate Research, Allégaten 55, 5007 Bergen, Norway. Tel.: +47 55584321; fax: +47 55584330.
E-mail address: bjorg.risebrobakken@bjerknes.uib.no (B. Risebrobakken).

0012-821X/$ - see front matter © 2005 Elsevier B.V. All rights reserved.
doi:10.1016/j.epsl.2005.11.032

differing boundary conditions. High-resolution TII records from a north–south transect along the eastern Nordic Seas are presented in order to answer these queries. The results are obtained from core MD99-2303 from the Fram Strait (77°31N, 08°24E: 2277 m water depth), MD95-2010 at the Vøring Plateau (66°41N, 04°34E: 1226 m water depth) and MD95-2009 in the Faeroe–Shetland Channel (62°44N, 03°59W: 1027 m water depth) (Fig. 1). All cores have been taken during IMAGES cruises on board the R. V. Marion Dufresne own by the French Polar Institute (IPEV).

The present oceanography in the Nordic Seas is influenced by the influx of warm, saline Atlantic water that flows northwards in the Norwegian Atlantic Current (NwAC) along the coast of Norway [10]. This current bifurcates and continues as the North Cape Current (NCC) and the West Spitsbergen Current (WSC) [11]. From the Arctic Ocean cold, less saline water enters the Nordic Seas through the Fram Strait, streaming southwards in the East Greenland Current (EGC). Deep winter convection and mixing of water masses occurs in the Greenland Sea and to a lesser extent in the Iceland Sea [12]. From the Greenland Sea, the deep bottom water currents can be traced in one northward flowing branch that reaches the Arctic through the eastern Fram Strait, and one southward flowing branch. The southward flowing bottom current is further split into one branch going south through the Faeroe–Shetland Channel and one branch turning north towards the Vøring Plateau (Fig. 1).

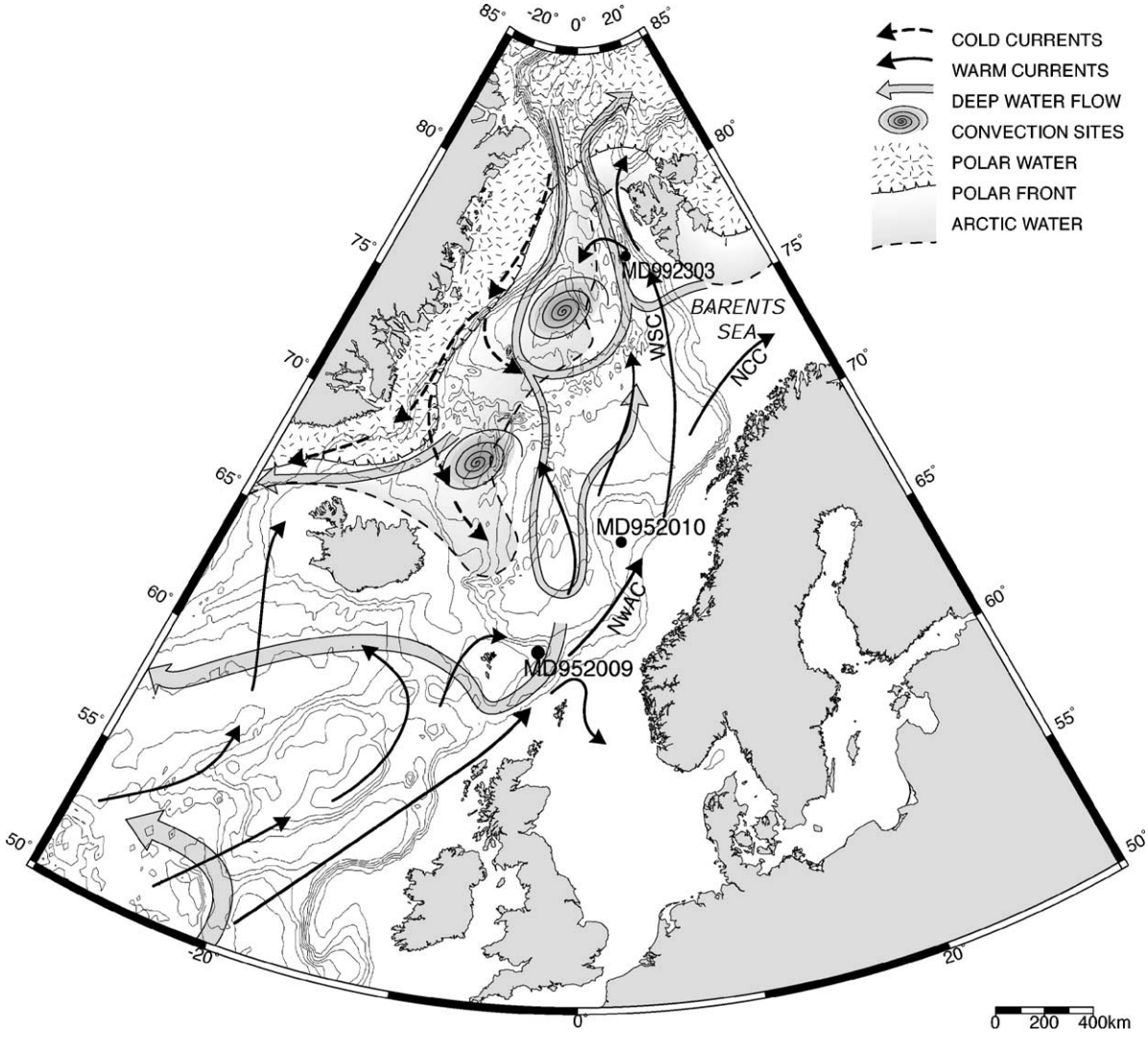

Fig. 1. Map showing the locations of the studied cores. The main oceanographic features of the region are indicated.

2. Methods

Stable isotopes were measured at the GMS laboratory in Bergen (MD99-2303 and MD95-2010) and at LSCE Gif-sur-Yvette (MD95-2009), using Finnigan MAT 251, 252 and Δ^+ mass spectrometers. Measurements were performed on the planktic foraminifer specie *Neogloboquadrina pachyderma* (sin), and on the benthic species *Oridorsalis umbonatus* (MD99-2303), *Cassidulina teretis* (MD95-2010) and *Melonis zaandamae* (MD95-2009). All results are reported in ‰ vs. VPDB. Benthic oxygen isotope values from *O. umbonatus* and *M. zaandamae* were corrected by +0.4‰ and +0.16‰, respectively, to account for departure from isotopic equilibrium [13,14]. *C. teretis* calcifies close to equilibrium [15], thus, no correction has been employed. Measurements were performed every cm if enough foraminifers were found in the samples. Where several measurements existed for one sample the mean of these measurements has been used.

Minerogenic grains >0.5 mm were counted in MD95-2010 and MD99-2303 and are considered to be ice rafted. These were counted every centimeter, and the records are presented as number of grains >0.5 mm/gram sediment. In MD99-2303 the grains were visually separated into sedimentary and crystalline components, to provide an indication on source regions of the ice rafted debris (IRD). The occurrence of chalk fragments in MD99-2303 was also registered, based on

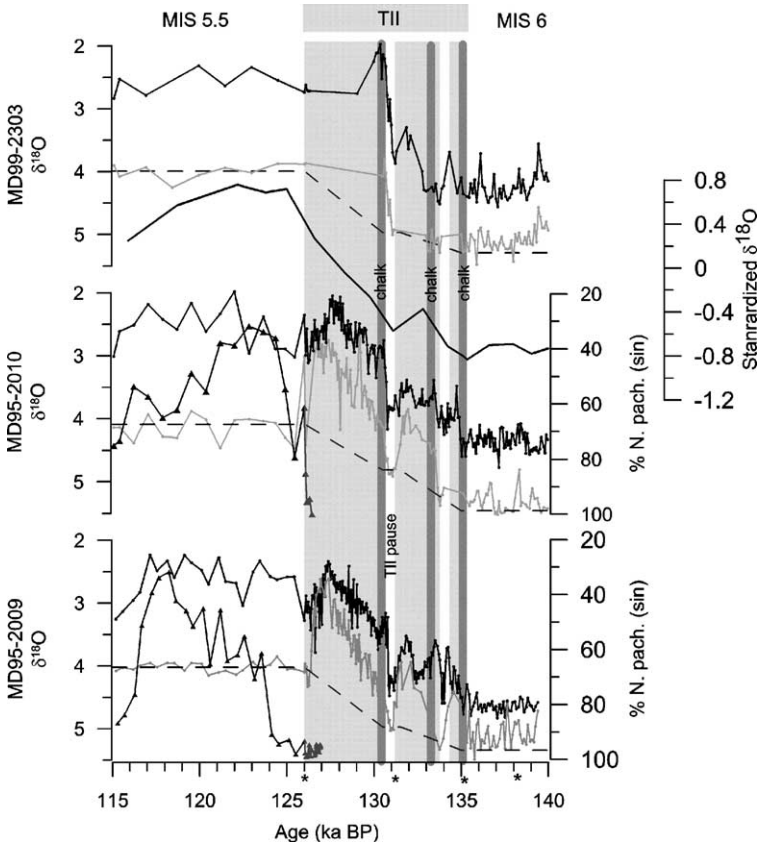

Fig. 2. Planktic and benthic δ^{18}O records from the studied cores are presented. All planktic records are performed on *N. pachyderma* (s) (black lines). The benthic measurements are performed on *O. umbonatus* (MD99-2303), *C. teretis* (MD95-2010) and *M. zandamae* (MD95-2009) (light grey lines). The dark grey lines (▲) show % *N. pachyderma* (sin) in MD95-2010 and in MD95-2009 (data from [19]). The stippled grey line represents the assumed δ^{18}O changes related to ice volume/sea level changes through the deglaciation for each core (based on Table 1). The maximum estimate is illustrated for MIS 6–TII pause interval. Oxygen isotope stages are indicated at the top. The light grey bars represent the melt water events found through the deglaciation/TII. Dark grey bars noted “chalk” indicate times when chalk fragments were deposited in the Fram Strait. The standardized δ^{18}O chronological framework from Martinson et al. [18] is shown for comparative reasons. Age control points are indicated by *'s. The age 126 ka BP represent the depths 935.5, 1262.5 and 1868 cm, 131.3 ka BP represents 1003.5, 1331.5 and 2158 cm, 135.1 ka BP represents 1037.5, 1383.5 and 2300 cm and 138.2 ka BP represents the depths of 1065.5, 1425.5 and 2371 cm in MD99-2303, MD95-2010 and MD95-2009, respectively.

visual identification, as these grains provide information on the source [16].

Low field volume magnetic susceptibility (χ_{lf}) were measured every second cm on u-channels, using a Bartington sensing coil with 4 cm diameter displaced along the u-channel section. All measurements were performed at the paleomagnetic laboratory at the LSCE in Gif-sur-Yvette. The magnetic susceptibility is presented as χ_{lf} (10–6 SI).

A Colortron handheld spectrophotometer was used to measure properties of the reflected light from the cleaned sediment surface of the archive part of MD99-2303. Measurements were performed every cm. The reflectance measurement provides the sediment colour in the L*a*b* colour difference system. L* is an indicator of the lightness of the sediment. Zero represents black, while 100 represents white. The lightness is assumed to be primarily related to the content of $CaCO_3$ in the sediment. However, at times, the lightness record is also influenced by the non-biogenic minerogenic composition of the sediment.

Semi-quantitative records of major and minor element composition were obtained by non-destructive X-ray fluorescence (XRF) logging with the CORTEX core-scanner [17]. Sample spacing was 2 cm. The Ca record, presented as counts per second (cps), is used as an indicator of the $CaCO_3$ content in the sediment.

3. Chronology

As a first approach to develop a common chronology, two tie points representing (1) marine isotope stage 6.2 (135.1 ka BP [18]) and (2) the onset of the last interglacial (126 ka BP) were identified in all three cores. The $\delta^{18}O$ records defined these tie points, and the % *N. pachyderma* (sin) records from MD95-2010 and MD95-2009 further support the interglacial start point. The age model of MD95-2010, defined by linear interpolation between these points, was then considered as a master chronology. In the next step, MD95-2009 and MD99-2303 were correlated towards the MD95-2010 age model by introducing two new tie points. The first of these tie points (131.3 ka BP) was defined by $\delta^{18}O$ correlation. The second (138.2 ka BP) was defined by correlating the χ_{lf} records. Age correlation points are indicated in Figs. 2 and 3. After these adjustments the chronologies are considered consistent for site-to-site comparison, and as independent as possible. The ages cannot be regarded as accurate absolute ages. The presented chronology of MD95-2009 was established independently of the previously published age model for this time interval in the core, and, thus, our age model differ in some aspects from the age model of Rasmussen et al. [19,20].

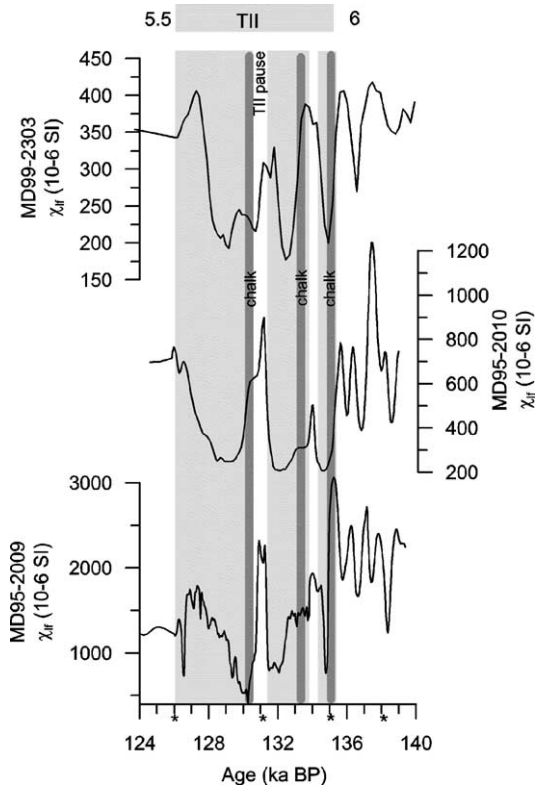

Fig. 3. Low field magnetic susceptibility records from all three cores. Oxygen isotope stages are indicated at the top. The light grey bars represent the melt water events found through the deglaciation/TII. Dark grey bars noted "chalk" indicate times when chalk fragments were deposited in the Fram Strait. Age control points are indicated by *'s.

The presented chronologies give mean sedimentation rates through the studied time span (139–126 ka BP) of 11 cm/ka for MD99-2303 (1073.5–935.5 cm), 15 cm/ka for MD95-2010 (1455.5–1262.5 cm) and 40 cm/ka for MD95-2009 (2390–1868 cm).

4. Results

Throughout late MIS 6, both planktic and benthic $\delta^{18}O$ show small-scale variability in the order of 0.5‰. Low $\delta^{18}O$ characterise the interval 135–131 ka BP (~1‰ change from the mean MIS 6 value), except for a brief event of high $\delta^{18}O$ at 134 ka BP (Fig. 2). At 131 ka BP a new, rapid, well-constrained $\delta^{18}O$ increase is seen in all three cores (~0.5–1‰). This reversal lasted for approximately one millennium before a new major rapid decrease occurred (~1–2‰). From this point onwards gradually decreasing values are recorded into the end of the termination (total of ~1‰) before a new

small increase of $\delta^{18}O$ appears towards the interglacial onset at 126 ka BP. A similar pattern is observed in both planktic and benthic $\delta^{18}O$ records throughout the studied time interval (Fig. 2).

All three cores show a relatively high degree of χ_{lf} variability, and the same main trends and events are found. Increased values are present just prior to the main $\delta^{18}O$ depletions, while during large parts of these events the χ_{lf} is rather low (Fig. 3). Both the Ca-content and the lightness record from MD99-2303 reflect the same type of variability as the χ_{lf} record, however with a slight time lag (Fig. 4). Thus, the

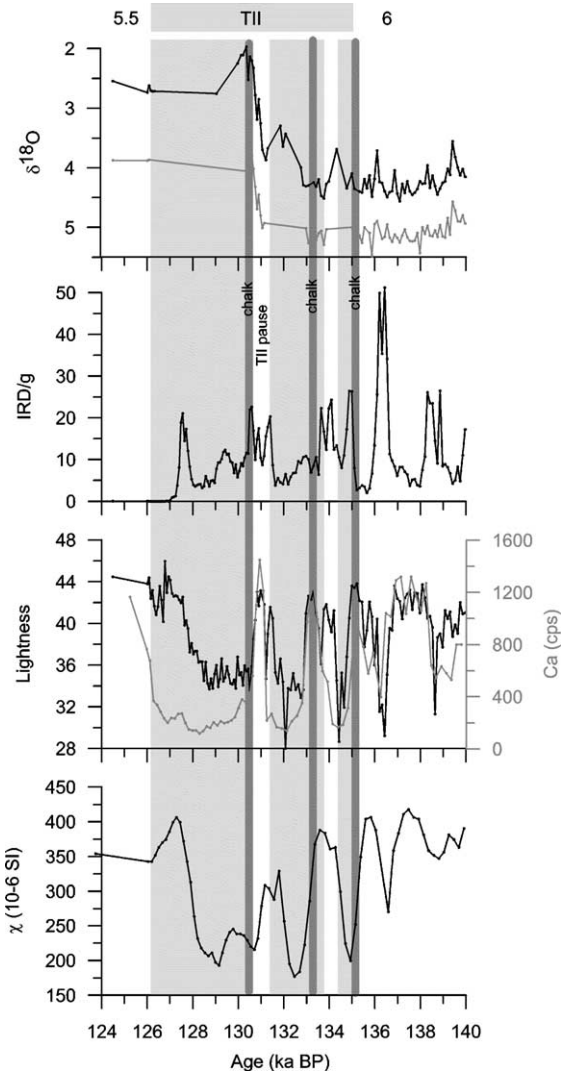

Fig. 4. Lightness (black line) and XRF Ca-content (cps) (grey line) of MD99-2303 is presented together with the low field magnetic susceptibility, IRD record and $\delta^{18}O$ records from the same core. The light grey bars represent the melt water events found through the deglaciation/TII. Dark grey bars noted "chalk" indicate times when chalk fragments were deposited in the Fram Strait.

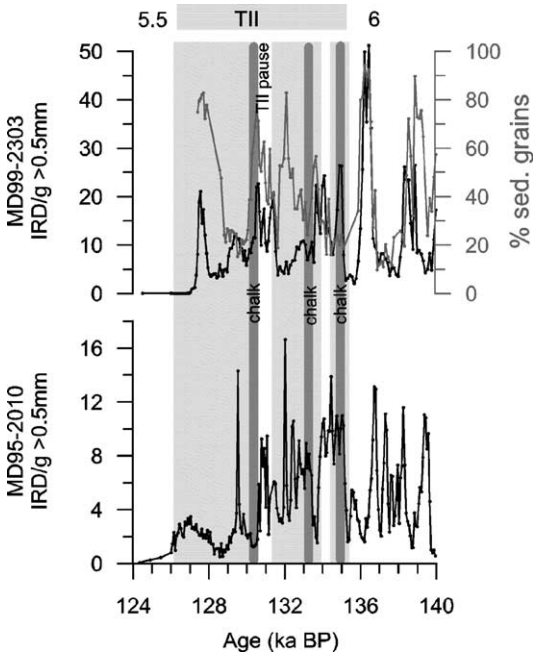

Fig. 5. Ice Rafted Debris (IRD) records from MD99-2303 (number of grains >0.5 mm/g sediment) and MD95-2010 (number of grains 0.5–1 mm/g sediment) are presented. For MD99-2303 the percentage of sedimentary grains >0.5 mm are also presented. Oxygen isotope stages are indicated at the top. The light grey bars represent the melt water events found through the deglaciation/TII. Dark grey bars noted "chalk" indicate times when chalk fragments were deposited in the Fram Strait.

lightness and Ca-content is high during periods of enriched planktic $\delta^{18}O$ while they are low during times of low $\delta^{18}O$ and increased IRD content in the sediment (Fig. 4). Therefore Ca-content cannot play the role of dilutant for the magnetic record.

Highly variable input of IRD is observed both at the Vøring Plateau and in the Fram Strait (Fig. 5). In the Fram Strait sedimentary grains generally dominate major IRD events. Times of low % sedimentary grains, and generally less IRD, in the Fram Strait, coincide with events of high IRD on the Vøring Plateau. Some chalk fragments (1–4 grains in each sample were chalk were present) are found in the Fram Strait during some of the Vøring Plateau high IRD events, generally just at the end of a high χ_{lf} event. In general, high IRD events concourse with low planktic and benthic $\delta^{18}O$ (Figs. 2 3 and 5).

5. Discussion

5.1. Proxy interpretation

When high IRD events (>10 grains/g sediment (>0.5 mm)) occur in the Fram Strait, there is a domi-

nance of sedimentary grains (>50%). This implies that the main IRD source was local, as the areas covered by the Svalbard–Barents Sea Ice Sheet (SBIS) primarily consists of sedimentary material [21]. Sometimes, an increased content of crystalline grains, together with small amounts of chalk fragments, is found in the Fram Strait sediment (Fig. 5). No source of chalk exists north of 59°N [16]. Thus, the presence of chalk in MD99-2303 requires a northward flowing current, drifting icebergs from the North Sea area to the Fram Strait. The high content of crystalline grains also indicate influence from a more distant source (Fig. 5). Major IRD input is found at the Vøring Plateau at these times, or just before, supporting an assumption of a southern IRD source. Northward chalk transport is seen towards the end of events of increased Ca-content and sediment lightness in MD99-2303 (Fig. 4). Both Ca-content and sediment lightness are considered related to the $CaCO_3$ concentration in the sediment [17,22]. Several aspects can influence the amount of $CaCO_3$ in marine sediments, e.g., variable production of $CaCO_3$ calcifying organisms, dilution due to increased influx of inorganic material or dissolution due to corrosive water masses [23]. As these events occur during periods with chalk evidence for northward flowing currents, we argue that the production of $CaCO_3$ probably increased due to the changing water mass properties.

Events of northward chalk transport together with increased lightness and Ca-content occur at the end of high χ_{lf} events in all three cores (Figs. 3 and 4). During MIS 3 high χ_{lf} in MD95-2009 and MD95-2010 corresponds with times of increased strength of the inflowing currents to the Nordic Seas, indicating a strengthened northern extension of the overturning circulation. Magnetic material was transported to the core sites from the basaltic ridges in the Iceland–Faeroe–Shetland area [24]. We assume that this relationship is valid also for the time period studied here. MD99-2303 is located close to the Knipovich Ridge, a mid-oceanic ridge system that may be a plausible source of magnetic material. The Knipovich Ridge directs the northward flowing branch of the deep water. If the overturning circulation and deepwater formation increases, the χ_{lf} signal of MD99-2303 should be influenced. The increase in the χ_{lf} signal found in all three cores, together with surface current transport northwards to the Fram Strait, indicates periods of enhanced northward extent of the AMOC. An increased strength of NwAC probably led to the increase in $CaCO_3$ content. The response in $CaCO_3$ is, however, somewhat delayed as compared to the initial response of the χ_{lf} signal.

5.2. Paleoceanographic changes through Termination II

At the end of MIS 6, the χ_{lf} data, in combination with the Ca-content and the lightness records, indicate a persisting overturning circulation, and thus increased influence of Atlantic water masses along the eastern Nordic Seas. This period of persistent overturning circulation was succeeded by a strong input of IRD at 135 ka BP. Contemporaneously with this enhanced IRD influx, planktic and benthic $\delta^{18}O$ show a marked decrease in MD95-2009, lasting to approximately 134 ka BP (Figs. 2 and 5). The planktic $\delta^{18}O$ depletion most probably results from the increased influence of freshwater as the icebergs melted. A freshening of the surface water may increase sea ice formation, thus increase the brine formation, and introduce low $\delta^{18}O$ to the bottom water [25,26]. The lack of measurements from MD99-2303 and MD95-2010 at this time, the result of to few foraminifers in the samples, supports the assumption of major brine formation. When brine is formed at the shelf it may, dependent on the source water conditions, get enriched in CO_2 [27]. This CO_2 enrichment makes the brine corrosive for $CaCO_3$, leading to increased dissolution of foraminifer tests. The effect of dissolution will also be specie dependent. *M. zaandamae* is more resistant to dissolution, because it lives deeper in the sediment [27]. Thus, depending on the overall site conditions, brine formation may be related to foraminifer barren sediment. The next and first major deglaciation step, approximately 134–131.5 ka BP, is also characterised by rather large IRD input and low planktic and benthic $\delta^{18}O$. Melt water and brine formation were probably the main factors influencing the $\delta^{18}O$ records. Also at this time a large foraminifer barren zone is seen in MD99-2303, probably related to the brine water. The conditions that initiated and characterised the second major melt water event, ~130.5–126 ka BP, also resemble the earlier melt water events, thus the same oceanographic mechanisms were probably operating (Figs. 2–5). The large input of freshwater to the Nordic Seas through these phases presumably weakened the northern limb of the AMOC as the stratification of the water masses increased. Such a weakening is indicated by the generally low χ_{lf} recorded through these intervals (Fig. 3), together with a low Ca-content and lightness (Fig. 4).

At 131 ka BP, a rapid expansion in the extent of the northern limb of the AMOC is indicated by the sharp increase in χ_{lf}, and supported by the increased Ca-content and lightness in MD99-2303 (Figs. 3 and 4). The circulation prevailed at a rather stable strong state

until about 130.5 ka BP. Through this approximately 1 ka long interval, both planktic and benthic $\delta^{18}O$ increased and stayed at a high level (Fig. 2). The high $\delta^{18}O$ indicate conditions less influenced by melt water and brine formation, and may represent a pause in the deglaciation. A deglacial pause at approximately this time has been documented in several previous studies [28–30]. In general, this pause has been considered a cold "Younger Dryas" like interval, with a reduced AMOC similar as during the rest of the deglaciation. The slowdown of the deglaciation and stability of global sea-level at this time [31] has also been used as an argument for generally cold conditions. Our records denote an enhanced overturning circulation through this interval and an increased northward extension of the NwAC. Thus, in contrast to the general climate deterioration, the eastern Nordic seas may have warmed slightly at this time. However, to constrain these implications, high-resolution SST reconstructions should be performed in all three cores. Foraminifer records from Rassmussen et al. [20] do show a slight decrease in the relative abundance of the polar specie *N. pachyderma* (sin) in MD95-2009 at this time.

Deepwater formation was probably maintained through melt water episodes by enhanced brine formation. Thus, some exchange of water masses between the Nordic Seas and the North Atlantic presumably took place throughout the penultimate deglaciation, even through the times characterised by a weakened northern AMOC limb. Similar conditions were present in the area during TI [32]. Veum et al. [32] argue that the deep-water formation was continuous throughout TI, at a reduced rate and with changing sources during the melt water events and comparable to the present day circulation through the Younger Dryas interval. A persistent communication between the Nordic Seas and the North Atlantic during TII has previously been put forward as a possible scenario [30], postulating the Nordic Seas as the source of North Atlantic intermediate water.

5.3. Sea level and temperature changes through Termination II

Superimposed on the $\delta^{18}O$ changes due to melt water and brine, there is an imprint due to a general temperature increase and a decreasing global ice volume/increasing sea level through the deglaciation. The temperature response in the Nordic Seas bottom water is considered small, as the present day interglacial bottom water temperature is close to the probable minimum in this area (Norwegian Sea Deep Water ~−0.5 °C [33]). During MIS 6, the TII pause at approximately 131 ka BP and MIS 5.5, the bottom water probably experienced a minimum brine influence. If these assumptions are correct, the deglaciation step from MIS 6 to the TII pause represents a benthic $\delta^{18}O$ change of 0.12–0.51‰ and the last step, TII pause to MIS 5.5, represent a benthic $\delta^{18}O$ change of 0.72–0.98‰ due to a reduced ice volume (Fig. 2, Table 2). Considering 0.11‰ to represent 10 m sea level [34], the total mean sea level change will be approximately 103 ± 6 m through the deglaciation (Table 2), a change somewhat lower than the previously estimated sea level change through TII (~130 m) [31]. Our estimated sea level change through the second deglaciation step (80 ± 13 m) is, however, in the same order of magnitude as a second major TII deglaciation step documented by coral records (sea level of -80 ± 10 m at 131 ± 2 ka BP) [31]. The MIS 6 mean is probably not representative for the glacial maximum level, possible due to small-scale brine influence (~0.5‰ variability is seen throughout MIS 6) (Fig. 2), thus giving to small changes through the first step. If the $\delta^{18}O$ mean of only the higher $\delta^{18}O$ from MIS 6 are considered (MD99-2303 > 5.2‰; MD95-2010 > 5.4‰ and MD95-2009 > 5.3‰), the total mean sea level change through TII is 121 ± 4 m, the first step representing 41 ± 16 m (Tables 1 and 2). These values are considered to be more reliable. A reduced deglacial $\delta^{18}O$ amplitude has also been recorded for TI in the Norwegian Sea [32].

In the planktic $\delta^{18}O$ records the residual signal after subtracting the ice volume effect will represent the SST change through the deglaciation, assuming negligible salinity changes during times of stronger AMOC. The change in SST from glacial maximum to interglacial conditions is largest in the Faeroe–Shetland Channel (estimated to 4 °C using the $\delta^{18}O$/temperature relation from [35]), decreasing further north (3.8 °C at the Vøring Plateau and 2.4 °C in the Fram Strait) (Table 2). This overall temperature change is considered a gradual response to the Northern Hemisphere summer insolation increase (Fig. 6).

5.4. Ice sheet disintegration

Just prior to the onset of the deglaciation the high χ_{lf}, Ca-content and lightness, and the occurrence of chalk fragments in the Fram strait sediment indicate an intensification of the northward flow of temperate surface waters. The deglaciation onset coincides with a significant oceanographic change. The northward surface branch of the AMOC experienced a marked weakening,

Table 1
Mean, maximum and minimum benthic and planktic $\delta^{18}O$ values for the intervals MIS 6 (values in parenthesis represent the higher MIS 6 level), the TII pause and MIS 5.5 are presented for the three studied cores

	Benthic			Planktic			
	Mean $\delta^{18}O \pm 1\sigma$	Maximum value	Minimum value	Mean $\delta^{18}O \pm 1\sigma$	Maximum value	Minimum value	Mean $\Delta\delta^{18}O$
MD99-2303							
MIS 6	5.09 ± 0.18 (5.29 ± 0,09)	5.48 (5.48)	4.57 (5.22)	4.24 ± 0.21	4.56	3.56	0.85
TII pause	4.97 ± 0.06	5.01	4.93	3.75 ± 0.11	3.87	3.67	1.22
MIS 5.5	3.99 ± 0.12	4.25	3.87	2.59 ± 0.20	2.83	2.32	1.4
MD95-2010							
MIS 6	5.32 ± 0.16 (5.46 ± 0.4)	5.52 (5.52)	4.80 (5.4)	4.63 ± 0.14	4.77	4.08	0.89
TII pause	4.81 ± 0.09	4.91	4.63	3.87 ± 0.15	4.17	3.63	0.94
MIS 5.5	4.09 ± 0.35	4.46	3.02	2.5 ± 0.31	3.02	1.98	1.56
MD95-2009							
MIS 6	5.10 ± 0.20 (5.34 ± 0,07)	5.49 (5.49)	4.61 (5.3)	4.63 ± 0.11	4.83	4.29	0.38
TII pause	4.97 ± 0.07	5.03	4.86	4.28 ± 0.10	4.47	3.17	0.69
MIS 5.5	4.02 ± 0.07	4.15	3.85	2.64 ± 0.31	3.28	2.23	0.74

The difference between the benthic and planktic $\delta^{18}O$ for the different time intervals are presented as $\Delta\delta^{18}O$.

shown by a marked decrease in χ_{lf}, Ca-content and lightness and low planktic and benthic $\delta^{18}O$ (Figs. 2–4). When the marine-based ice sheets reached the shelf edge during maximum MIS 6 glaciation [36–38], the relatively warm surface water probably increased the melt-rates. The warming associated with increased Northern Hemisphere summer insolation (Fig. 6) would also enhance the melting. In combination, these conditions may have had a destabilising effect on the ice sheet [39,40], thus initiating major iceberg calving (Fig. 5). The validity of grounding line instability mechanisms for marine ice sheets has been questioned [41], however, the general understanding of related mechanisms is still rather limited. As major calving is indicated in relation to and immediately after the event of enhanced AMOC just before 135 ka BP (Fig. 5), we argue that this circulation change was probably important for the initiation of the penultimate deglaciation. A present day study indicates that ocean heat may be important for major disintegration events of an Antarctic ice shelf [42]. Thus, ocean heat transport can be considered as a plausible mechanism for initiating major ice sheet disintegration. The onset of calving and ice sheet melting involved a slight sea level

Table 2
The benthic $\delta^{18}O$ change, sea level change, planktic $\delta^{18}O$ change, the residual between planktic and benthic change (planktic residual) and the temperature change is presented for the interval between MIS 6 and the TII pause at approximately 131 ka BP (Step 1), the interval between the TII pause and MIS 5.5 (Step 2), and for total deglaciation (MIS 6 to MIS 5.5) for all three cores

		MD99-2303	MD95-2010	MD95-2009	Mean change
Step 1 (MIS6–TII pause)	Benthic $\delta^{18}O$ change	0.12‰ (0.32‰)	0.51‰ (0.65‰)	0.13‰ (0.37‰)	0.25 ± 0,22‰ (0.45 ± 0.18‰)
	Sea level change	11 m (29 m)	46 m (59 m)	12 m (34 m)	23 ± 20 m (41 ± 16 m)
	Planktic $\delta^{18}O$ change	0.49‰	0.76‰	0.35‰	0.53‰
	Planktic residual	0.37‰	0.25‰	0.22‰	0.28‰
	Temperature change	1.6 °C	1.1 °C	1 °C	1.2 °C
Step 2 (TII pause–MIS5.5)	Benthic $\delta^{18}O$ change	0.98‰	0.72‰	0.95‰	0.88‰
	Sea level change	89 m	66 m	86 m	80 ± 13 m
	Planktic $\delta^{18}O$ change	1.16‰	1.34‰	1.64‰	1.38‰
	Planktic residual	0.18‰	0.62‰	0.69‰	0.50‰
	Temperature change	0.8 °C	2.7 °C	3 °C	2.2 °C
Total deglacial change	Benthic $\delta^{18}O$ change	1.10‰	1.23‰	1.08‰	1.14‰
	Sea level change	100 m (118 m)	112 m (125 m)	98 m (120 m)	103 ± 6 m (121 ± 13 m)
	Planktic $\delta^{18}O$ change	1.65‰	2.1‰	1.99‰	1.91‰
	Planktic residual	0.55‰	0.87‰	0.91‰	0.78‰
	Temperature change	2.4 °C	3.8 °C	4 °C	3.4 °C

The mean of the different parameters for the three cores is also presented. Values in parenthesis represent the results if only the mean of the highest MIS 6 values are used in the calculations.

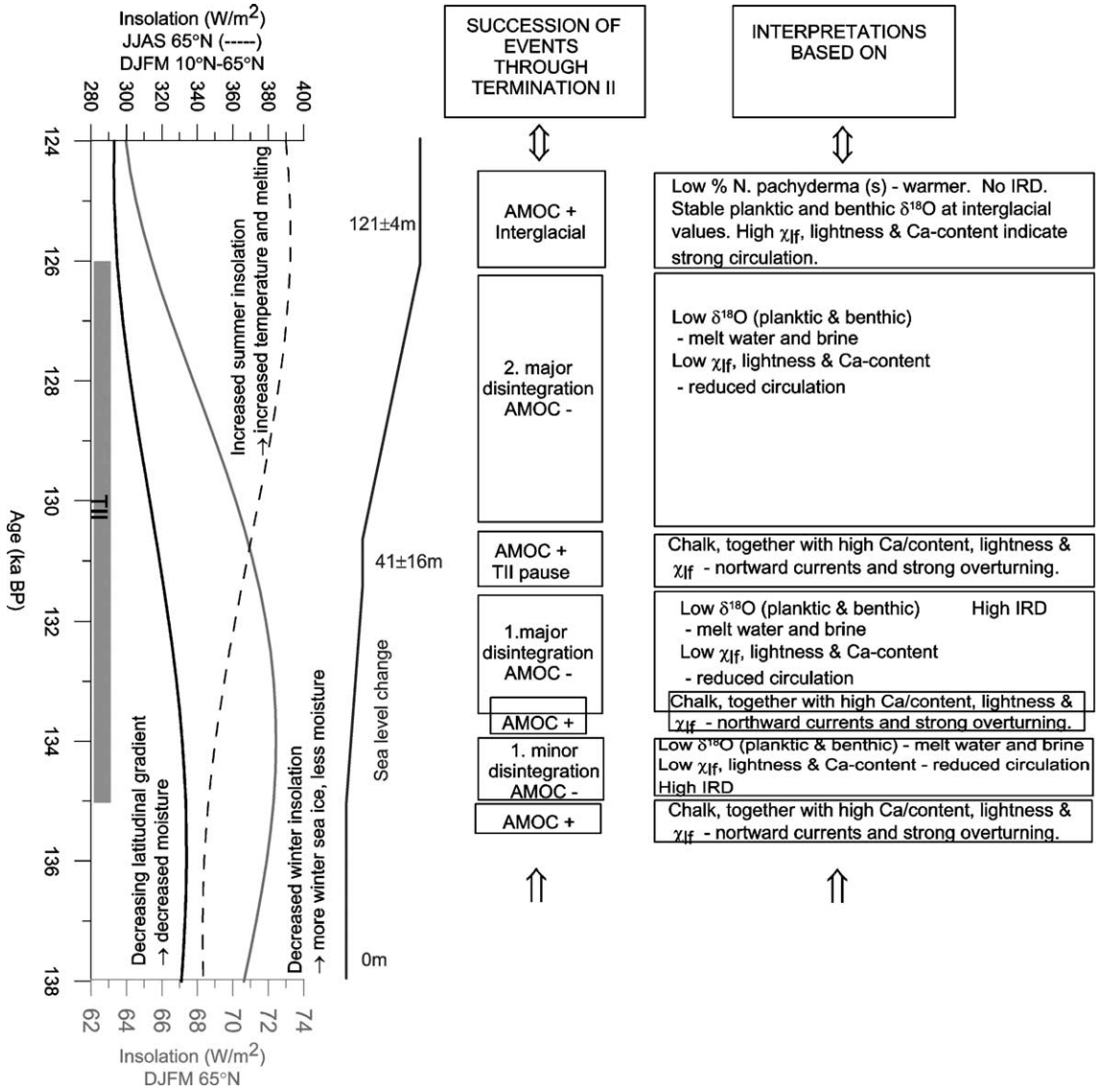

Fig. 6. Summer insolation at 65°N (stippled line), winter insolation at 65°N (grey line) and winter season insolation gradient between 10°N and 65°N (black line). All insolation data are from Laskar [48]. The grey bar indicates the deglaciation phase. The sea level change through TII, as calculated in this study, is indicated. The succession of events found to characterize TII is indicated, as well as cues to what the interpretations are based on.

increase. Such a sea level rise probably acted as a possible feedback on the deglaciation, by further destabilising the ice sheets [39,40]. This mechanism was active for all the disintegration steps.

5.5. Interactions

The initial triggering mechanism for the TII onset is still not known. A combination of several boundary conditions reaching a threshold more or less at the same time, and the effect of feedback mechanisms connected to these changes was probably crucial. The presented records show that the amplification of the NwAC was important for the initiation of the disintegration of the Northern European ice sheets. A strong NwAC initiated a stronger northward salt and heat flux, and rapidly enhanced the northern limb of the overturning circulation. This entailed the first major melt water event observed in the Nordic Seas. The release of huge amounts of fresh water further perturbed the overturning and weakened the circulation. Sea level changes related to the major melting further destabilised the ice

sheets. Also the subsequent deglaciation steps were influenced by this mechanism. Thus, TII were characterized by a succession of periods of stronger and weaker AMOC, and how these variations introduced major melting/calving of the vulnerable marine based ice sheets (Fig. 6). Eventually the final major reorganisation of the AMOC occurred, introducing strong interglacial overturning circulation conditions from 126 ka BP. Our records cannot tell us what caused the rapid reorganisations that lead to enhanced AMOC. It has, however, been suggested that the mechanism initiating a strong circulation after times of weakened overturning is connected to build up of surplus heat and salt in the tropical Atlantic during times of weak overturning [43].

The large amounts of cold fresh water masses that were introduced during the melt water events entailed intensive sea ice formation during the winter season, amplified by the decreasing winter insolation through TII (Fig. 6). Intensive wintertime sea ice formation decreased the moisture transport to the ice sheets [23]. However, not only direct moisture flux, or lack of it, from the nearby oceans is of significance for the disintegration process. The meridional moisture flux, driven by the latitudinal insolation gradient, is also of major importance [44]. During TII, a low winter time latitudinal insolation gradient existed (Fig. 6) [8,45]. A weaker insolation gradient during winters resulted in fewer and less intensive low pressure storm systems, less precipitation, more cloud-free days, increased absorption of solar radiation in the ice and thus increased summer melting [8]. Further, the summertime ablation increased due to the gradual increasing Northern Hemisphere summer insolation (Fig. 6). A combination of lowered winter accumulation and intensified summer ablation introduced a negative mass balance of the ice sheets [23]. Thus, an interaction between several feedback mechanisms that worked together, probably lead to the total disintegration of the penultimate glacial state. The oceanographic changes as well as sea level rise, moisture starvation, increased insolation and albedo were probably all factors of importance.

5.6. Termination II vs. Termination I

Comparing our TII $\delta^{18}O$ results from MD95-2010 with the TI $\delta^{18}O$ records from the same core [26], indicates distinct similarities between these two deglaciation events (Fig. 7). Both terminations are characterised by two major melt water events with major brine formation. The first major melt water event during TII can be considered an analogue to H1. Similarly, the interval from 131.5–130.5 ka BP, where our results indicate stable northward heat transport in the northern limb of the AMOC, can be compared with the Bølling–Allerød time period, followed by a Younger Dryas like interval, before going into the final major deglaciation/melt water event. Some similarities can also be seen between the IRD and susceptibility records, however, not as clear as for the oxygen isotopes (Fig. 7). The fact that the two deglaciations differ in the details should,

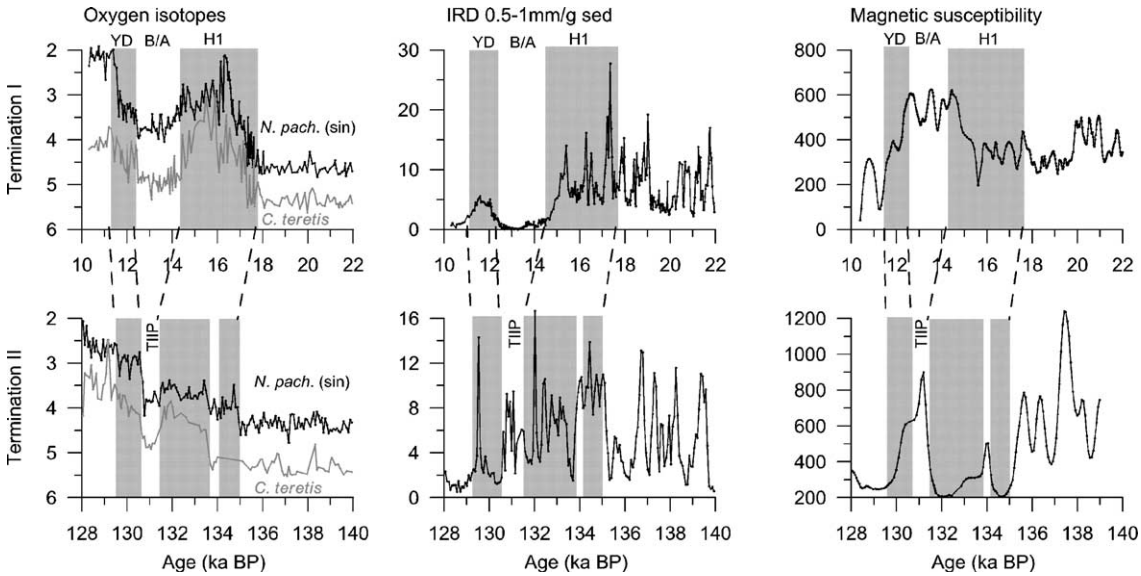

Fig. 7. Planktic and benthic $\delta^{18}O$, χ_{lf} and IRD records from TII in MD95-2010 are shown together with and compared to similar records covering TI in the same core [26]. The TII pause (TIIP) and the melt water events are indicated in the TII records. The Younger Dryas (YD), Bølling–Alerød (B/A) and Heinrich 1 (H1) events are indicated for TI.

however, not be surprising. The different boundary conditions (e.g., insolation and ice sheet extension) would tend to produce differences in some aspects. Thus, the records from MD95-2010 give some support to previous arguments for a similar succession of events through TII and TI [29,30,46,47]. It is therefore reasonable to consider that some of the same mechanisms operate in both deglaciations.

6. Summary and conclusions

The penultimate deglaciation of the Northern European Ice Sheets occurred in a stepwise manner. One initial minor melt water event was followed by two major melt water events. During these events, the northern limb of the AMOC was weakened. Due to massive brine formation a continuous deep-water formation were, however, maintained at a reduced rate. The melt water events were separated by and initiated after times of strong overturning and northward heat transport. The warmer water influenced the stability of the ice sheets and entailed melting and calving. As the ice sheets melted, the sea level increased and further destabilised the ice sheets. The calculated sea level change through TII, based on the presented records, were 121 ± 4, 41 ± 16 m in the first part of the deglaciation, 80 ± 13 m in the last part. Contemporaneously, the winter moisture flux to the ice sheets decreased, due to a decreasing winter insolation and a decreasing latitudinal wintertime insolation gradient. The increasing high latitude summer insolation increased the melting through the summer season. Thus, through time there was an over all negative mass balance. As the ice sheets retreated, the albedo decreased and further amplified the effect of the increasing high latitude summer insolation. The confluence of changing boundary conditions for all these different factors of importance was probably essential for the final disintegration of the northern European ice sheets. Comparing TII with TI show some clear similarities between the two deglaciation events.

Acknowledgements

We thank Dag Inge Blindheim, Grethe Blindheim, Rune Søraas and Odd Hansen for laboratory assistance. We also thank Ulysses S. Ninnemann for comments on the language and content of an early version of the paper. All studied cores were provided through the IMAGES program on board the R.V. Marion Dufresne. The crew and the captain are fully thanked for their help in getting the cores. The magnetic measurements and interpretation were made at LSCE using the softwares developed by A. Mazaud. This study was supported by a University of Bergen/Bjerknes Centre fellowship to B.R. We thank two anonymous reviewers for their useful comments that significantly improved the manuscript. This is publication Nr A117 from the Bjerknes Centre for Climate Research.

References

[1] M.E. Raymo, The timing of major climate transitions, Paleoceanography 12 (4) (1997) 577–585.
[2] J. Imbrie, A. Berger, E.A. Boyle, S.C. Clemens, A. Duffy, W.R. Howard, G. Kukla, J. Kutzbach, D.G. Martinson, A. McIntyre, A.C. Mix, B. Molfino, J.J. Morley, L.C. Peterson, N.G. Pisias, W.L. Prell, M.E. Raymo, N.J. Shackleton, J.R. Toggweiler, On the structure and origin of major glaciation cycles: 2. The 100,000-year cycle, Paleoceanography 8 (6) (1993) 699–735.
[3] J. Imbrie, E.A. Boyle, S.C. Clemens, A. Duffy, W.R. Howard, G. Kukla, J. Kutzbach, D.G. Martinson, A. McIntyre, A.C. Mix, B. Molfino, J.J. Morley, L.C. Peterson, N.G. Pisias, W.L. Prell, M.E. Raymo, N.J. Shackleton, J.R. Toggweiler, On the structure and origin of major glaciation cycles: 1. Linear responses to Milankovitch forcing, Paleoceanography 7 (6) (1992) 701–738.
[4] R.B. Alley, P.U. Clark, The deglaciation of the northern hemisphere, Annu. Rev. Earth. Planet. Sci. 27 (1999) 149–182.
[5] G.A. Jones, L.D. Keigwin, Evidence from Fram Strait (78°N) for early deglaciation, Nature 336 (1988) 56–59.
[6] W.H. Berger, E. Jansen, Mid-Pleistocene climate shift—the Nansen connection, the polar oceans and their role in shaping the global environment, Geophys. Monogr. 84 (1994) 295–311.
[7] W.F. Ruddiman, A. McIntyre, The North Atlantic Ocean during the last deglaciation, Palaeogeogr. Palaeoclimatol. Palaeoecol. 35 (1981) 145–214.
[8] R.G. Johnson, Major Northern Hemisphere deglaciation caused by a moisture deficit 140 ka, Geology 19 (1991) 686–689.
[9] W.R. Peltier, S. Marshall, Coupled energy-balance/ice-sheet model simulations of the glacial cycle: a possible connection between terminations and terrigenous dust, J. Geophys. Res. 100 (D7) (1995) 14269–14289.
[10] K.A. Orvik, P. Niiler, Major pathways of Atlantic water in the northern North Atlantic and Nordic Seas toward Arctic, Geophys. Res. Lett. 29 (19) (2002) 1896.
[11] T. Furevik, Annual and interannual variability of Atlantic water temperatures in the Norwegian and Barents Sea: 1980–1996, Deep-Sea Res. I 48 (2001) 383–404.
[12] K. Aagaard, J.H. Swift, E.C. Carmack, Thermohaline circulation in the Arctic Mediterranean Seas, J. Geophys. Res. 90 (C3) (1985) 4833–4846.
[13] D.W. Graham, B.H. Corliss, M.L. Bender, L.D. Keigwin Jr., Carbon and oxygen isotopic disequilibria of recent deep-sea benthic foraminifera, Mar. Micropaleontol. 6 (1981) 483–497.
[14] D.A.R. Poole, Neogene and Quaternary paleoenvironment on the north Norwegian shelf, PhD thesis, Institute of Biology and geology, University of Tromsø, 1994.
[15] E. Jansen, U. Bleil, R. Henrich, L. Kringstad, B. Slettemark, Paleoenvironmental changes in the Norwegian Sea and the Northeast Atlantic during the last 2.8 m.y.: Deep Sea Drilling Project/Ocean Drilling Program Sites 610, 642, 643 and 644, Paleoceanography 3 (5) (1988) 563–581.

[16] D. Hebbeln, T. Dokken, E.S. Andersen, M. Hald, A. Elverhøi, Moisture supply for northern ice-sheet growth during the Last Glacial Maximum, Nature 370 (1994) 357–360.
[17] J.H.F. Jansen, S.J. Van der Gaast, B. Koster, A.J. Vaars, CORTEX, a shipboard XRF-scanner for element analyses in split sediment cores, Mar. Geol. 151 (1998) 143–153.
[18] D.G. Martinson, N.G. Pisias, J.D. Hays, J. Imbrie, T.C. Moore Jr., N.J. Shackleton, Age dating and the orbital theory of the ice ages: development of a high-resolution 0 to 300,000-year chronostratigraphy, Quat. Res. 27 (1987) 1–29.
[19] T. Rasmussen, E. Balbon, E. Thomsen, L. Labeyrie, T.C.E. van Weering, Climate records and changes in deep outflow from the Norwegian Sea ~150–55 ka, Terra Nova 11 (2/3) (1999) 61–66.
[20] T.L. Rasmussen, E. Thomsen, A. Kuijpers, S. Wastegård, Late warming and early cooling of the sea surface in the Nordic seas during MIS 5e (Eemian Interglacial), Quat. Sci. Rev. 22 (2003) 809–821.
[21] A. Elverhøi, E.S. Andersen, T. Dokken, D. Hebbeln, R. Spielhagen, J.I. Svendsen, M. Sørflaten, A. Rørnes, M. Hald, C.F. Forsberg, The growth and decay of the Late Weichselian Ice Sheet in Western Svalbard and adjacent areas based on provenance studies of marine sediments, Quat. Res. 44 (1995) 303–316.
[22] J. Ortiz, A. Mix, S. Harris, S. O'Connell, Diffuse spectral reflectance as a proxy for percent carbonate content in North Atlantic sediments, Paleoceanography 14 (2) (1999) 171–186.
[23] W.F. Ruddiman, B. Molfino, A. Esmay, E. Porkas, Evidence bearing on the mechanism of rapid deglaciation, Clim. Change 3 (1980) 65–87.
[24] C. Kissel, C. Laj, L. Labeyrie, T. Dokken, A. Voelker, D. Blamart, Rapid climatic variations during marine isotopic stage: 3. Magnetic analysis of sediments from Nordic Seas and North Atlantic, Earth Planet. Sci. Lett. 171 (1999) 489–502.
[25] H. Craig, L.I. Gordon, Deuterium and oxygen 18 variations in the ocean and the marine atmosphere, in: E. Tomgiorgi (Ed.), Stable Isotopes in the Oceanographic Studies and Paleotemperatures, Cons. Naz. Delle Ric. Lab. Di Geol. Nucl., Pisa, 1965, pp. 9–130.
[26] T.M. Dokken, E. Jansen, Rapid changes in the mechanism of ocean convection during the last glacial period, Nature 401 (1999) 458–461.
[27] P.I. Steinsund, M. Hald, Recent calcium carbonate dissolution in the Barents Sea: paleoceanographic applications, Mar. Geol. 117 (1994) 303–316.
[28] A. Lototskaya, G.M. Ganssen, The structure of Termination II (penultimate deglaciation and Eemian) in the North Atlantic, Quat. Sci. Rev. 18 (1999) 1641–1654.
[29] M.-S. Seidenkrantz, L. Bornmalm, S.J. Johnsen, K.L. Knudsen, A. Kuijpers, S.E. Lauritzen, S.A.G. Leroy, I. Mergeal, C. Schweger, B. Van Vliet-Lanoë, Two-step deglaciation at the oxygen isotope stage 6/5e transition: the Zeifen–Kattegat climate oscillation, Quat. Sci. Rev. 15 (1996) 63–75.
[30] D.W. Oppo, L.D. Keigwin, J.F. McManus, J.L. Cullen, Persistent suborbital climate variability in marine isotope stage 5 and Termination II, Paleoceanography 16 (3) (2001) 280–292.
[31] M.T. McCulloch, T. Esat, The coral record of last interglacial sea levels and sea surface temperatures, Chem. Geol. 169 (2000) 107–129.
[32] T. Veum, E. Jansen, M. Arnold, I. Beyer, J.C. Duplessy, Water mass exchange between the North Atlantic and the Norwegian Sea during the past 28,000 years, Nature 356 (1992) 783–785.
[33] J. Blindheim, Arctic Intermediate Water in the Norwegian Sea, Deep-Sea Res. 37 (9) (1990) 1475–1489.
[34] N.J. Shackleton, N.D. Opdyke, Oxygen isotope and palaeomagnetic stratigraphy of Equatorial Pacific Core V28-238: oxygen isotope temperatures and ice volumes on a 105 year and 106 year scale, Quat. Res. 3 (1973) 39–55.
[35] N.J. Shackleton, Attainment of isotopic equilibrium between ocean water and the benthonic foraminifera genus *Uvigerina*: isotopic changes in the ocean during the last glacial, Colloq. Int. Centre Natl. Rech. Sci. 219 (1974) 203–209.
[36] J. Mangerud, T. Dokken, D. Hebbeln, B. Heggen, Ó. Ingólfsson, J.Y. Landvik, V. Mejdahl, J.I. Svendsen, T.O. Vorren, Fluctuations of the Svalbard–Barents sea ice sheet during the last 150,000 years, Quat. Sci. Rev. 17 (1998) 11–42.
[37] J.I. Svendsen, H. Alexanderson, V.I. Astakhov, I. Demidov, J.A. Dowdeswell, S. Funder, G. Gataullin, M. Henriksen, C. Hjort, M. Houmark-Nielsen, H.W. Hubberten, Ó. Ingólfsson, M. Jakobsson, K.H. Kjær, E. Larsen, H. Lokrantz, J.P. Lunkka, A. Lysså, J. Mangerud, A. Matiouchkov, A. Murray, P. Möller, F. Nisessen, O. Nikolskaya, L. Polyak, M. Saarnisto, C. Siegert, M.J. Siegert, R.F. Spielhagen, R. Stein, Late Quaternary ice sheet history of northern Eurasia, Quat. Sci. Rev. 23 (2004) 1229–1271.
[38] J. Mangerud, E. Jansen, J.Y. Landvik, Late Cenozoic history of the Scandinavian and Barents Sea ice sheets, Glob. Planet. Change 12 (1996) 11–26.
[39] R.H. Thomas, The dynamics of marine ice sheets, J. Glaciol. 24 (90) (1979) 167–177.
[40] C.R. Warren, Iceberg calving and the glacioclimatic record, Prog. Phys. Geogr. 16 (3) (1992) 253–282.
[41] R.C.A. Hindmarsh, E. Le Meur, Dynamical processes involved in the retreat of marine ice sheets, J. Glaciol. 47 (157) (2001) 271–282.
[42] A. Shepard, D. Wingham, T. Payne, P. Skvarca, Larsen Ice Shelf has progressively thinned, Science 302 (2003) 856–859.
[43] C. Rühlemann, S. Mulitza, P.J. Müller, G. Wefer, R. Zahn, Warming of the tropical Atlantic Ocean and slowdown of thermohaline circulation during the last deglaciation, Nature 402 (1999) 511–514.
[44] M.E. Raymo, K. Nisancioglu, The 41 kyr world: Milankovitch's other unsolved mystery, Paleoceanography 18 (1) (2003) 1011.
[45] M.A. Young, R.S. Bradley, Insolation gradients and the paleoclimatic record, in: A. Berger, J. Imbrie, J. Hays, G. Kukla, B. Saltzman (Eds.), Milankovitch and Climate: Part 2. NATO ASI Series, vol. 126, D. Reidel Publishing Company, 1984, pp. 707–713.
[46] M. Sarnthein, R. Tiedemann, Younger Dryas-style cooling events at glacial terminations I–VI at ODP Site 658: associated benthic δ^{13}C anomalies constrain meltwater hypothesis, Paleoceanography 5 (6) (1990) 1041–1055.
[47] A. Lototskaya, P. Ziveri, G.M. Ganssen, J.E. van Hinte, Calcareous nannofloral response to Termination II at 45° N, 25° W (northeast Atlantic), Mar. Micropaleontol. 34 (1998) 47–70.
[48] J. Laskar, The chaotic motion of the solar system: a numerical estimate of the chaotic zones, Icarus 88 (1990) 266–291.